Graphene and 2D Materials (2023) 8:151–159
https://doi.org/10.1007/s41127-023-00064-4

ORIGINAL ARTICLE

Revealing enhanced X-Ray radiation shielding of 2D layered materials and their laminar heterostructures

Le Yu[1] · Md J. Nine[1] · Tran T. Tung[1] · Ana L. C. Pereira[1,2] · Kamrul Hassan[1] · Diana Tran[1] · Alexandre Santos[3,4,5] · Dusan Losic[1]

Received: 17 June 2023 / Revised: 6 September 2023 / Accepted: 8 September 2023 / Published online: 13 October 2023

Abstract

This paper demonstrates a new concept of using two-dimensional (2D) layered materials and their heterostructures for enhanced X-ray radiation shielding. This phenomenon is revealed by characterization on the X-ray shielding performances of several 2D materials with high atomic numbers (Z), including MoS_2, antimonene (Sb), and MXene prepared as multi-layered and heterostructure films by assembly their few-layer sheets. Results showed considerable X-ray shielding enhancement of (40–50%) at 30 kVp for individual 2D multi-layered films compared with their bulk structures of these materials. Furthermore, when these multi-layered films were combined into laminar heterostructures structures (e.g., MoS_2 + MXene), further enhancement of 60% was achieved. The mechanism of the observed X-ray shielding enhancement by these multi-layered 2D structures is not clear at this stage. It is postulated to be the result of an additional multiple scattering and reflections of photons between multiple layers of 2D crystals inside the film, which does not occur in their uniform bulk materials. The presented results suggest that multi-layered 2D materials with high atomic numbers (Z) and their laminar heterostructures could offer a new and promising strategy for designing of a new generation of Pb-free radiation-shielding materials, which is urgently needed across broad sectors.

Graphical abstract

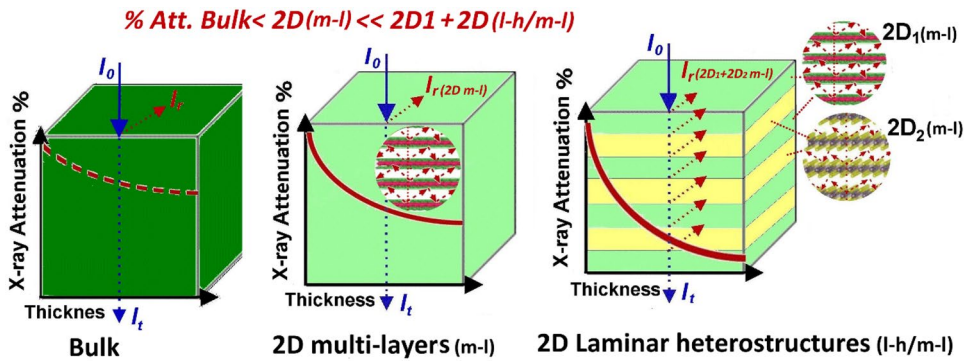

Keywords 2D materials · Multi-layered structure · Heterostructures · X-rays shielding

1 Introduction

There is a growing demand for improving protection from the exposure to ionising radiations such as X-rays used across the broad sectors including medical, mining, nuclear, military and space industry [1]. To protect operators from overexposure to hazardous X-rays, an efficient, low-cost, affordable, and efficient radiation shielding materials are needed [2]. Medical irradiation used in diagnostics is considered as one of the largest artificial sources of radiation exposure, which is of great concern to human health [1, 2]. Protective metallic lead (Pb) in different forms such as foils, plates, bricks, glass, and Pb-based garments is

Extended author information available on the last page of the article

conventionally used for X-ray protection, as Pb is able to block and absorb most of the radiation [1, 3–6]. However, Pb-based materials have many disadvantages, such as being extremely heavy, uncomfortable to wear, toxic, non-disposable, and environmentally unsustainable [6, 7]. It is significant to develop a new generation of lightweight, non-toxic, and sustainable Pb-free radiation shielding materials that comply with the international standards for X-ray radiation protection.

To achieve these goals, several materials with high atomic numbers (Z) and densities, such as tin (Sn), antimonene (Sb), tungsten (W), and bismuth (Bi) and their combination, have been explored as potential Pb alternatives [8–11]. Most of these materials were prepared in the forms of polymer-based composites, but also as the films, and fabrics showing promising shielding performances [12, 13]. Although polymer-based composites have been widely used for the formation of lightweight Pb-free X-ray shielding materials, the pinholes and voids within the composites have a negative effect on X-ray attenuation, as the incident X-rays can easily pass through these voids [1]. To address this issue, the use of materials with a densely packed structures in the film forms proved to be more desirable and able to reduce the penetration of incident X-rays. To improve the performance of X-ray shielding films, the studies from several groups including ours have shown that using metal oxide forms with high atomic numbers (Z) with nano-scale dimensions with high surface-to-volume (SA/V) ratios can provide enhanced shielding performance [14–16]. This is because the high SA/V nanomaterials are homogenously dispersed in the film to create a densely packed layer. These results also indicate that by designing the internal architecture of the material, it is possible to further enhance their radiation-shielding performance compared to their bulk structures.

Since the debut of graphene in 2004, the 2D materials have received their designation as "materials of the twenty-first century" owing to their unique monoatomic 2D structures and outstanding properties, including physical, chemical, electrical, optical, magnetic, thermal, mechanical, etc. [17]. They have opened new horizons in materials science and engineering to create novel materials, properties, and devices for a broad range of applications [18]. It was recently discovered that the combination of two or more 2D materials in the form of the laminated structures could generate more intriguing properties, which are different from their single-layer structures [19, 20]. This opens unprecedented opportunities for new discoveries and applications using 2D layered structures [21, 22]. Following these studies, it is reasonable to expect that layered and laminated structures of 2D materials may have different effects on the radiation-shielding properties across the broad electromagnetic range [23–25]. Molybdenum disulfide (MoS_2) has a high Z of 42 with a high density of 5.06 g/cm^3, which potentially makes it ideal as a radiation shielding material. A study by Vogl et al. showed gamma-radiation tolerance of 2D materials such as hBN and MoS_2 has been used for the device protection in space explorations [24]. The applications of 2D layered materials such as graphene and MXene were reported for electromagnetic interference shielding (EMI) owing to their unique layered structure [25–28]. It is also reported that the merit of MXene is to offer the feasibility of manufacturing flexible (bendable and foldable) thin films for the effective radiation shielding, providing the benefit for generation of the flexible X-ray protective garments. Moreover, the first study presented from our group showed that laminated 2D antimonene (Sb) had an efficient shielding against X-ray radiation, indicating the increased probability of X-ray scattering and interaction can improve X-ray shielding ability [29].

Inspired by these studies, this paper presents that experimental demonstration of new concept based on the multi-layered and laminar heterostructures of 2D materials can significantly enhance X-ray shielding. This phenomenon is illustrated in Fig. 1 showing SEM image and scheme of 2D multi-layered structures with the proposed interactions of X-rays compared with their bulk materials. The X-ray shielding by these 2D structure is explained to be a result of the multiple scattering and interactions (reflection)

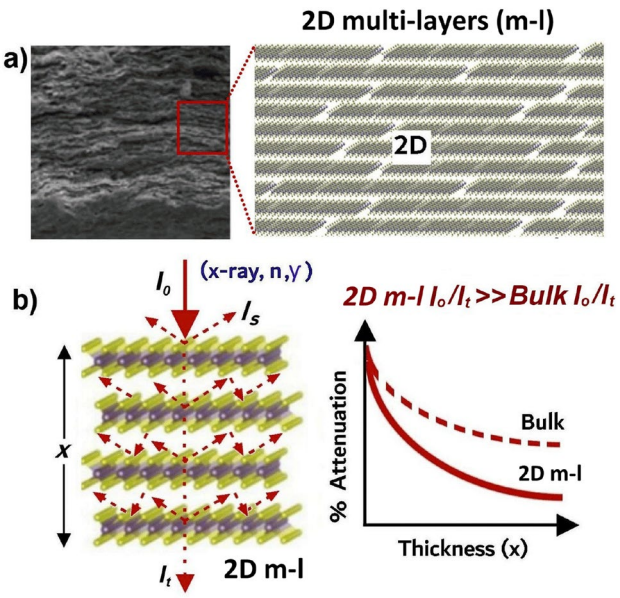

Fig. 1 **a** Cross-sectional SEM images showing typical 2D structure of the film created by self-assembly of 2D nanosheets, which are schematically presented on the right. **b** Schematic illustration of the interaction between X-ray photons and the multi-layered structure of 2D crystals, showing multiple scattering occurred between each layer causing a significant X-ray shielding ability that is not observed in bulk material. The enhancement of X-ray attenuation by 2D multi-layered is presented on the right graph showing comparison with corresponding bulk material with the same thickness (or mass of material)

of the photons occurring at the top and interface between each layer in multi-layered structure, leading to significant shielding results that is not observed in the bulk structures. Considering the unique structural properties of 2D material films by the self-assembly of their 2D crystal sheets into multiple layers, each layer could act as a shielding barrier that reduces the photon energy by multiple internal scattering and absorption. We believe this shielding concept is universal and can be applied for shielding other ionizing radiation (gamma-rays, neutron). To demonstrate this X-ray shielding concept by 2D multi-layered, we prepared these films using several different 2D materials with high atomic Z numbers, such as MoS_2, antimonene (Sb), and MXene. The films were made by self-assembly of their nanosheets with few atomic layers prepared by a common exfoliation process. In addition, laminar heterostructures were created by combining two or more individual multi-layered films, such as MoS_2 + MXene to explore their impact on shielding properties. The X-ray shielding performance at a low-energy X-ray (30 kVp) was investigated for all prepared films (experimental set-up Figure S1), compared with that of their complementary films composed of bulk structures using the same mass.

2 Experimental

2.1 Chemicals and materials

Molybdenum disulfide powder (MoS2, 99.99%, 23 µm) and sodium bromide (NaBr) was purchased from Chem-Supply (Australia). Bulk crystalline antimonene (Sb) with 99.9% purity was purchased from Smart Elements, Austria. The Ti_3AlC_2 (MAX) was supplied by Carbon-Ukraine. Carboxymethylcellulose sodium salt (CMC, high viscosity) and isopropanol (reagent grade, ≥ 99.5%) were provided by Sigma-Aldrich (Australia).

2.2 Preparation of 2D materials

Bulk MoS_2 powder was exfoliated into single layer MoS_2 sheets using a Planetary Ball Mill PM 200 (Retsch, Australia) with zirconium balls (3 mm in diameter) [30]. NaBr was added to facilitate the process of the ball milling with a weight ratio of NaBr/MoS_2 at 20:1, and the weight ratio of balls to powder was also 20:1. After the dry ball milling process (18 h), NaBr in the as-prepared mixture was removed by washing several times using distilled (DI) water with the aid of a centrifuge (Sigma, Australia, 4200 rpm) and then, dried in oven at 50 °C overnight for the further step.

The synthesis steps of 2D MXene nanosheets was performed followed a literature guideline [23, 28, 31]. Briefly, the small pieces of Ti_3C_2Tx MAX phase were ground into fine powders using a mortar, and the powders having a particle size of less than 25 µm were selected by a 25 µm sieve and collected for further use. Lithium fluoride (1.5 g) was added to 20 ml of 9 M HCl solution in a reaction vessel under and stirred with a magnetic bar, then 1 g of Ti_3C_2Tx was slowly added into the solution. The mixture was maintained in an oil bath environment at 35 ºC for 24 h. After the etching reaction was completed, the reacted mixture was subjected to centrifugal washing with deionized (DI) water at 3500 rpm for 30 min. This washing procedure was repeated 5 to 6 times until the pH value reached around 6, and a relatively pure Ti_3C_2Tx (MXene) was obtained. After washing, the product was ultrasonically separated to obtain a two-dimensional layered MXene material. A small amount of MXene powder was obtained by drying the raw MXene material, and its dispersion was filtered to make a film for sheet resistance and then calculated electrical conductivity.

Few-layer antimonene (FL-Sb) nanosheets were prepared in a 4:1 isopropanol/water mixture by exfoliating bulk Sb crystals using a combination of ball milling and ultrasonication [29]. Bulk Sb crystals were put in a zirconia milling pot with isopropanol/water solvent. The samples were then ball-milled using Retsch planetary ball mill (PM 200) with zirconia balls (1 mm) at 300 rpm for 30 min. After drying, the ball-milled Sb flakes (30 mg) were re-dispersed in 4:1 isopropanol/water mixture (10 mL) for further exfoliation. The exfoliation was carried out in a bath ultrasonication for 40 min. Then, the resulting black suspension was centrifuged at 3000 rpm for 3 min, and the dark grey supernatant was recovered.

2.3 Preparation of 2D multi-layered films and their laminar heterostructures

Few-layer exfoliated MoS_2 were dispersed with DI water and then bath-sonicated for 1 h, respectively. CMC solution (0.5 wt%) was added to the as-prepared MoS_2 solution with the optimized weight ratio to prepare dispersion with known MoS_2 concentration of 10 mg/ml. The mixture was then stirred constantly for 3 h at the room temperature (20 ± 2 °C) followed by composed of multi-layered structures of assembled MoS_2 sheets via vacuum filtration. The prepared MoS_2 film was then dried for 12 h in air at the room environment (20 ± 2 °C) and used as a freestanding film for X-ray experiments. The mass loading and thickness of the film were measured to be consistent with prepared films using other 2D materials.

The MXene films were produced by the same method of vacuum filtration as following details using MXene dispersion in deionized water that was sonicated for 1 h before filtration. Required volumes (2 ml to 8 mL) of as-prepared MXene solutions were slowly filtrated by a vacuum filtration system to form MXene layered films on the membranes. The

MXene-deposited membrane connected to the suction filter was placed in a vacuum drying oven and dried at 40ºC for 12 h. After that, the entire system was taken out from the vacuum drying oven, the suction filter was removed, and then, the dried MXene film was carefully separated from the membrane and used for X-ray measurements.

Similar process was applied to make 2D antimonene multi-layered films using prepared 2D FL-Sb dispersion with known concentration and volume to achieve with the same mass loading as 2D MoS_2 and 2D MXene films. Double laminar heterostructure films were self-assembled by stacking individually prepared 2D MoS_2 layered film and 2D MXene layered film into one combined structure (MoS_2/MXene). Quadrupole laminar heterostructure films were followed the same method by double stacking individual 2D MoS_2 layered films and individual 2D MXene layered films into one combined structure (MoS_2/MXene/MoS_2/MXene).

2.4 Characterizations

A scanning electron microscope (SEM-FEI Quanta 450, Japan) in a low vacuum chamber at an accelerating voltage of 5 kV. The average thickness and particle topography of exfoliated FL-Sb was examined using an NT-MDT Ntegra Solaris Atomic Force Microscope (AFM) via tapping mode. NT-MDT SPM Software (Nova 1.0.26) was used for AFM image processing. A particle size analyser from Malvern instrument (NanoSight NS300) was used to examine the average particle size distribution. A transmission electron microscope (TEM, FEI Titan Themis) was used to acquire nanoscale morphology and elemental analysis of exfoliated substances. Thermogravimetric analysis (TGA) of FL-Sb, PDMS and their composite were studied using Mettler-Toledo TGA/DSC 2, Switzerland in an air atmosphere at a constant heating rate of 5 °C/min. The vibrational stretching modes of different molecular bonds in PDMS modified samples were studied by Fourier transform infrared spectroscopy (FTIR) (Nicolet 6700 Thermo Fisher, USA).

2.5 X-ray radiation measurements

X-ray transmission testing was performed using a superficial X-ray tube (SXR) unit (Gulmay D3150, UK) as shown in Figure S7. The distances between the X-ray tube and sample-placing panel and sample-placing panel to the detector were equally 50 cm. This setup was selected as it produces a scatter free and narrow-beam arrangement, recommended internationally for the measurement of half-value layers in materials. The samples were exposed to the X-ray voltage range at 30, 50, 80, 100 kVp, respectively, for 0.50 min with the X-ray transmitted sample placing area of diameter at 1 cm, and the X-ray attenuation performance was evaluated as the transmission dose of samples divided by the transmission dose without the sample. Each sample was measured 3 times and determined by the arithmetic mean. The X-ray attenuation of an X-ray beam is expressed as a function of the linear attenuation coefficient (μ) and calculated using equation and procedure as reported elsewhere.

3 Results and discussion

3.1 Fabrication and characterization of prepared multi-layered structures of 2D materials

A comprehensive characterisation on physical, chemical and thermal properties of the synthesized few-layers MoS_2 sheets, antimonene and MXene and their layered films are summarized in Fig. 2 and Figure S2-S4. A ball-milling method was employed to exfoliate a large quantity of micron sized MoS_2 sheets with an average particle size of 22 μm (Figure S2) into few-layers nanosheets with an average particle size of 432 nm (Figs. 2a and S2). The corresponding SEM and TEM image (Fig. S2a and Fig. 2a) confirmed the presence of the sheet-like MoS_2 structure with significant changes in their particle size and morphology. High-resolution TEM images showed the exfoliated MoS_2 nanosheet with ~ 7 layers (inset of Fig. 2a**.** Raman, XRD, and FTIR analyses (Fig. S2) confirming their significant differences from that of bulk MoS_2.

Few-layers MXene was prepared using a common etching process from Ti_3C_2Tx MAX phase materials as described in the literature [25, 26]. Their typical structure characterized by SEM and TEM was presented in Fig. 2b, and Figure S2 confirmed a few-layer structure of MXene with the dimension of a few hundred nanometers. Few-layer 2D antimonene (FL-Sb) nanosheets were synthesized by exfoliating bulk Sb crystals, and the structural differences before and after exfoliation were summarized in Figs. 2c and S3. The exfoliation of bulk-Sb (30–45 μm, Figure S3a) transformed into the nanosheets (confirmed by TEM in Figs. 2c and S3c) with an average lateral dimension ranging between 300 and 400 nm (confirmed by particle size distribution Fig. S3d). Figure S3e presented the powder diffraction pattern of exfoliated FL-Sb nanosheets showing a typical signature of Sb nanopowder, which was in good agreement with the standard diffraction card "JCPDS no. 01-085-1324". These 2D sheet structures dispersed in a solution were used to fabricate their multi-layered films using a vacuum filtration process. During this process, 2D sheets were self-assembled into a layered film structure, and their typical cross-sectional SEM images were presented in Fig. 2d–f. These images clearly confirmed the formation of their layered film structure composed of thousands of layers assembled 2D sheets, which was assumed to have a strong Van Der Waals interaction between each layer. It is worth nothing that these layered

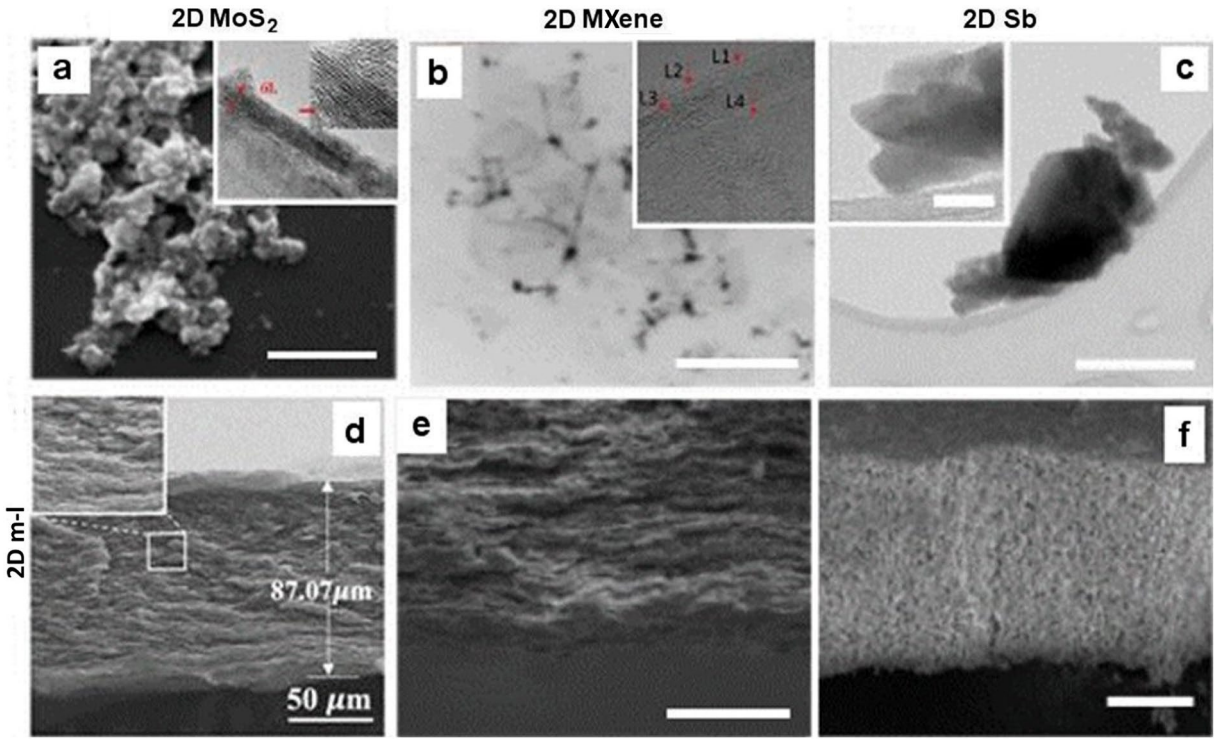

Fig. 2 **a** SEM and TEM images of the exfoliated nanosheets from the selected 2D materials a) SEM images of 2D MoS_2 nanoplatelets (scale bar = 1 μm). **b** TEM images of 2D MXene nanosheets showing their few layers structure (inset), **c** TEM images of 2D antimonene (Scale bar = 100 nm) with inset confirming few layers structure. Cross-sectional SEM images of the prepared films confirming their multi-layered structure **d** MoS_2, **e** MXene (scale bar = 50 μm) and **f** antimonene (scale bar = 50 μm)

films can be prepared with the controllable thickness from tens to several hundreds of microns including making their heterostructure films by combining different 2D materials.

3.2 X-Ray shielding performance of multi-layered structures of 2D materials

The study on X-ray transmission and the attenuation enhancement of the prepared individual 2D MoS_2, MXene and antimonene layered films compared to their corresponding bulk films was presented in Fig. 3 and Table S1. These results showed a significant decrease in the X-ray

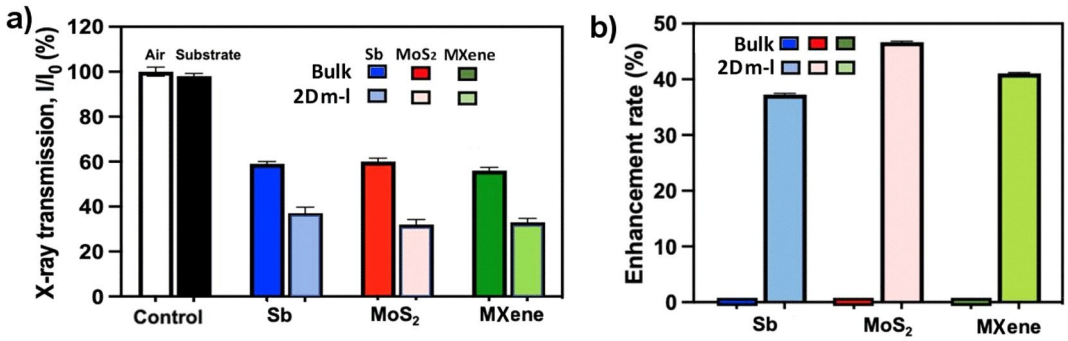

Fig. 3 Comparative X-ray transmission results performed at 30 kVp showing **a** difference in X-ray shielding performance between multi-layered films of selected 2D materials composed of self-assembled 2D sheets of MoS_2, Sb and MXene and their control bulk structures; **b** the X-ray attenuation enhancement rate in % of layered 2D films compared to their bulk films. All tested materials were used with the same mass loading in the film and measurements performed in triplicate

transmission of the 2D layered films at 30 kVp, compared to their bulk counterparts. Figure 3b confirmed that the X-ray attenuation enhancement rates of 46.67% for MoS_2 film, 37.28% for 2D antimonene and 41.07% for MXene film were achieved compared to their bulk films. It is worth noting that the mass loading of all the prepared films including controls had a similar mass (g/m^2). The results obtained at a lower X-ray energy of 30 kVp were presented where the X-ray attenuation enhancement difference is the most significant and relevant. However, the X-ray transmission measurements at the higher energy of 50 kVp and 80 kVp were also performed as the same trend but with lower shielding enhancement (data not shown), indicating that this phenomenon is more prominent at lower energies. To improve the shielding performance at higher energies, a combination with other materials should be considered.

It is well known that that X-ray shielding is dependent on the thickness of the material. By increasing the thickness of these 2D multi-layered films, it will be possible to further improve their performances. This optimization was further demonstrated by controlling the film thickness in case of MoS_2 layered films prepared with different thickness or masses per surface area. Figure S5 presented the X-ray transmission results, showing that by increasing their thickness of the MoS_2 films from 0.11 mm to 1.34 mm this could effectively attenuate the X-ray transmission down to 0.09%. The X-ray transmission value of the exfoliated MoS_2 film with the optimized thickness of 1.34 mm was further evaluated compared with 0.20 mm Pb sheet indicating comparable performance to 0.20 mm Pb-equivalent attenuation at 30 kVp (inset of Fig. S5). Although the optimized thickness (1.34 mm) of layered 2D MoS_2 film was much thicker than the 0.20 mm Pb sheet, the weight of this film (minus the holding substrate) at 1.18 g was 50% lighter than the 0.20 mm Pb (2.17 g). This can be defined as outstanding results that are comparable to Pb benchmark materials, indicating layered 2D materials could be a promising solution for the development of new generation of lightweight and Pb-free shielding materials for broad protection applications.

3.3 X-Ray shielding performance of multi-layered and laminar heterostructures

In the following experiment, the X-ray radiation shielding performance of the films with multi-layered and laminar heterostructure of 2D materials prepared by combining two or more individual multi-layered films such as MoS_2 and MXene was explored. One combination of these double laminar multi-layered films was made using the MoS_2 film on the top and the MXene film on the bottom (MoS_2/MXene). The second was composed of the MoS_2 and MXene films subsequently ordered as quadruple laminar heterostructures (MoS_2/MXene/MoS_2/MXene). Comparison of the obtained X-ray transmission results on these films was presented in Fig. 4. The results showed that the double laminar heterostructures increased X-ray shielding enhancement towards their individual multi-layered for 12.85% MoS_2 and 6.62% MXene with the same mass loading, respectively. However, the films with quadruple laminar heterostructure multi-layered films showed further significant shielding ability of 62.26% for MoS_2 and 59.57% for MXene compared to their films composed of individual multi-layers. By changing the orientation of these laminates as either MXene film on the top or MoS_2 film on top, there was no difference observed. This is due to the fact that photoelectric effect is dominant interaction at low-energy X-ray, its probability mainly depends on Z and thickness of the shielding materials. With the increasing number of laminates from 2 to 4, it significantly increases probability of photoelectric effect by providing the additional X-ray absorption and scattering

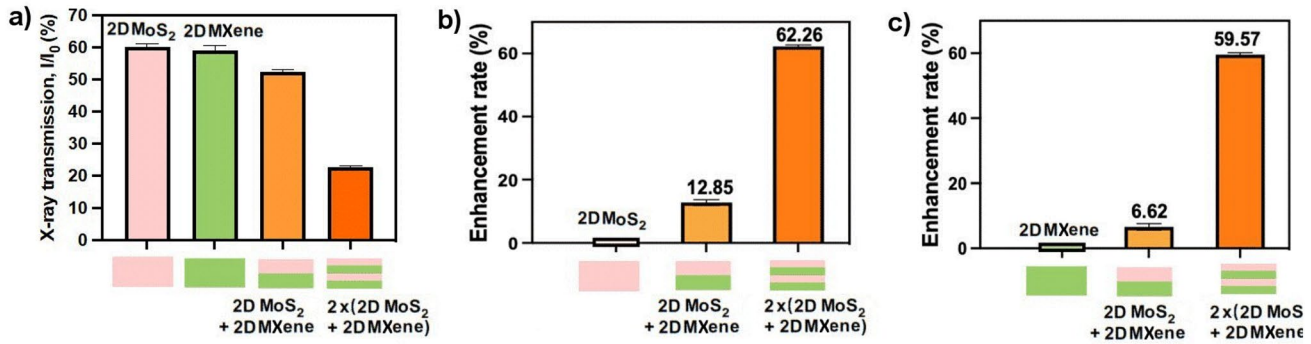

Fig. 4 X-ray transmission results performed using 2D multi-layered materials and their laminar heterostructures combined by MoS_2 and MXene in the forms of double (MoS_2/MXene) and quadruple (MoS_2/MXene/MoS_2/MXene) films; **b** the enhancement rate of multi-layered laminar heterostructures compared to individual 2D MoS_2 layered film, and **c** the enhancement rate of multi-layered heterostructures compared to individual 2D MXene layered film. All tested materials were used with the same mass loading, and an X-ray shielding experiment was performed at 30 kVp and measurements in triplicate

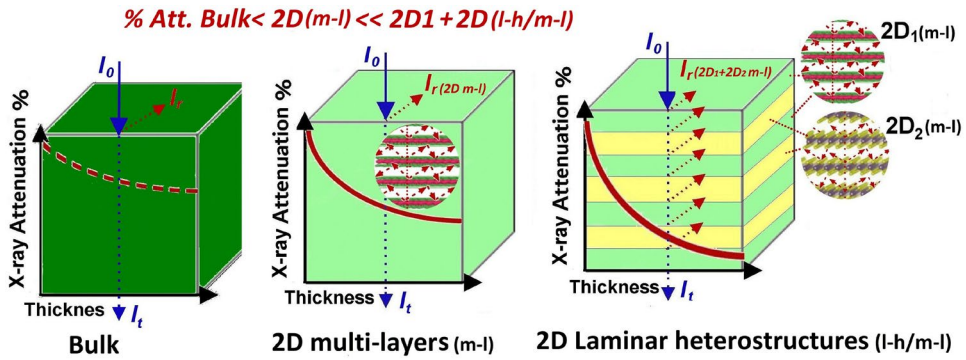

Fig. 5 The schematic illustration to explain a significant enhancement of X-ray attenuation or reduction in X-ray transmission (I_t) on individual 2D multi-layered materials (m-l) and their heterolaminar structures (ml + hl) with corresponding bulk structure. This enhancement is presented as results of increased internal scattering of photons inside 2D layers which significantly reduce their transmission through the structure compared to uniform bulk material. The % of X-ray attenuation caused by scattering between each layer inside multi-layered film (ml) composed on of individual 2D material (1) is further enhanced by additional scattering at the interface (I) when the film is composed with the heterolaminar architecture with two 2D (2) layered materials (ml)

between the interfaces of each layer [31]. However, more studies are needed to understand the mechanism of these enhancements by heterostructures. These results suggests that increasing number of laminates of the 2D multi-layered films could further enhance shielding performance. This is another promising strategy to further improve the X-ray shielding performance, which deserves to be explored in the future work.

These presented results clearly reveal experimental evidence that multi-layered 2D materials, and their laminar heterostructures can enhance X-ray shielding. To provide theoretical validation of this experimental evidence, we try to perform the Monte Carlo simulation used for modelling of X-ray attenuation of bulk materials. However, our attempt to perform theoretical simulation by the Monte Carlo simulation to predict these properties was not very successful. Main reason was the high complexity of the model to describe the multi-layered and laminar heterostructures of 2D materials used in our study. So far, the current physical models can only consider the uniform bulk structure. There has been no simulation model for the interaction with multi-layered 2D structures, as shielding is dependent on parameters such as Z atomic number, density and the film thickness. The complexity of this model is related to consideration of many parameters such as the size and morphology of individual 2D crystal sheets, number of their atomic layers, their crystallinity, number, layers in the film, their interlayer distances, Van Der Waals interactions between layers, the interfaces between laminated structures, and number of laminates, etc. Moreover, the interaction of X-ray photons inside these multi-layered structures is reasonable to be different from that of the bulk structure of material. We expect that these models will be developed in the future enabling to theoretically verify the experimental results presented in this paper and predict how to improve the design of more optimized heterostructures and their combinations.

The X-ray attenuation is known as the process of the X-ray intensity reduction via either absorption or scattering when X-ray photons pass through the shielding material [1, 2]. It involves three interaction mechanisms including (1) photoelectric effect, (2) Compton scattering, and (3) pair production [27]. To explain the observed attenuation results of the 2D layered materials, we assumed that the X-ray shielding performance could be enhanced because of multiple scattering and absorption occurred when the incoming X-ray photons that interacted with these layered films. This type of scattering process is less relevant within the bulk materials, where most of the deflection occurred on the top surface, as schematically presented in Fig. 1. The multi-layered 2D material films can increase the probability of photoelectric effect within each layer in the film, leading to enhanced X-ray shielding ability. In other words, incident X-ray is absorbed and reflected many times between each layer (+ 1000 layers) within the layered 2D material films, making their attenuation properties much higher compared to non-layered and bulk materials. In terms of the combination of two or more 2D layered films and their heterolaminar structures, the multiple interfaces between each layer of the 2D laminates will provide additional scattering and absorption of X-ray photons multiple times as shown in Fig. 5. This is a reasonable explanation for the observed shielding enhancement, but more studies are needed to fully reveal the mechanism of X-ray interactions within these 2D layered heterostructures and establish their appropriate models to predict these interactions for a range of high-Z 2D materials .

4 Conclusions

In summary, the presented study practically demonstrates that the multi-layered films composed of 2D materials such as MoS_2, MXene and antimonene and their laminar heterostructures can significantly attenuate low-energy (30 kVp) X-ray. The phenomenon is explained as a result of the multiple scattering and absorption inside the 2D multi-layered film structures that is not observed in bulk material. The X-ray shielding enhancement of 46.67% for layered MoS_2, 37.28% for antimonene and 41.07% for MXene was determined compared with their bulk counterparts. Surprisingly, further enhancement of X-ray shielding was achieved by a heterostructure (double and quadruple laminates) generated from the combination of individual films such as MoS_2 and MXene, showing 62.26% and 59.57% compared to their individual MoS_2 and MXene layered films. This paper presents an exciting discovery about X-ray shielding properties of 2D materials and their heterostructures, which is not considered before. This finding will also open a new horizon for designing a new Pb-free radiation shielding technology and its successful application across the broad sectors in medicine, nuclear industry, space exploration, and defence. Further studies on the theoretical modelling based on photon interactions with 2D multi-layered structures are needed to give more insights for understanding this mechanism, facilitating the development of more advanced shielding structures.

Supplementary Information The online version contains supplementary material available at https://doi.org/10.1007/s41127-023-00064-4.

Acknowledgements The authors acknowledge the financial support from the ARC Research Hub for Graphene Enabled Industry Transformation, (IH150100003). We thank Australian Microscopy for the access of SEM, TEM facilities, Mr. Ken Neubauer, Dr. Ashley Slattery for their technical support on SEM and TEM measurements.

Author contributions L. Y: Synthesis, Investigation, Methodology, Formal analysis, Validation, drafting and editing, Md J. N.: Investigation, Methodology, Validation, Editing, T. T. T: Investigation, data processing, Editing A. C. P: Simulation study, data analysis, Editing K. H: Investigation, data processing, Editing D. T: Editing, co-Supervision A. S: Methodology, Data analysis, Editing D. L: Conceptualization, Methodology, writing—original draft, Resources, Supervision, Editing, Submission

Funding Open Access funding enabled and organized by CAUL and its Member Institutions.

Declarations

Conflict of interest The authors declare that they have no conflict of interest.

References

1. Podgorsak EB (2016) Radiation physics for medical physicists. Springer, Berlin
2. Noz ME, Maguire GQ (1999) Radiation protection in health sciences. World Scientific, New York
3. Hughes JS, Watson SJ, Jones AL, Oatway WB (2005) Review of the radiation exposure of the UK population. J Radiol Prot 25(4):493. https://doi.org/10.1088/0952-4746/25/4/010
4. ICRP (2020) Radiological protection of people and the enviroment in the event of a large nuclear accident, vol 4
5. McCaffrey JP, Mainegra-Hing E, Shen H (2009) Optimizing non-Pb radiation shielding materials using bilayers. Med Phys 36(12):5586–5594
6. Needleman H (2004) Lead poisoning. Annu Rev Med 55:209–222
7. Kim Y, Park S, Seo Y (2015) Enhanced X-ray shielding ability of polymer–nonleaded metal composites by multilayer structuring. Ind Eng Chem Res 54(22):5968–5973. https://doi.org/10.1021/acs.iecr.5b00425
8. Wang Y, Zhong R, Li Q, Liao J, Liu N, Joshi NS, Guo J (2020) Lightweight and Wearable X-Ray Shielding Material with Biological Structure for Low Secondary Radiation and Metabolic Saving Performance. Adv Mater Technol 5(7):2000240
9. Kadyrzhanov KK, Shlimas DI, Kozlovskiy AL, Zdorovets MV (2020) Research of the shielding effect and radiation resistance of composite CuBi 2 O 4 films as well as their practical applications. J Mater Sci: Mater Electron 31:11729–11740
10. Maghrabi HA, Vijayan A, Mohaddes F, Deb P, Wang L (2016) Evaluation of X-ray radiation shielding performance of barium sulphate-coated fabrics. Fibers and Polymers 17:2047–2054
11. Nambiar S, Yeow JT (2012) Polymer-composite materials for radiation protection. ACS Appl Mater Interfaces 4(11):5717–5726. https://doi.org/10.1021/am300783d
12. Li Q, Wang Y, Xiao X, Zhong R, Liao J, Guo J, Shi B (2020) Research on X-ray shielding performance of wearable Bi/Ce-natural leather composite materials. J Hazard Mater 398:122943
13. Nambiar S, Osei EK, Yeow JT (2013) Polymer nanocomposite-based shielding against diagnostic X-rays. J Appl Polym Sci 127(6):4939–4946. https://doi.org/10.1002/app.37980
14. Verdipoor K, Alemi A, Mesbahi A (2018) Photon mass attenuation coefficients of a silicon resin loaded with WO3, PbO, and Bi2O3 Micro and Nano-particles for radiation shielding. Radiat Phys Chem 147:85–90
15. Yu L, Pereira AL, Tran DN, Santos AM, Losic D (2021) Bismuth oxide Films for X-ray shielding: effects of particle size and structural morphology. Mater Chem Phys 260:124084. https://doi.org/10.1016/j.matchemphys.2020.124084
16. Yu L, Yap PL, Santos A, Tran D, Losic D (2021) Lightweight bismuth titanate (Bi4Ti3O12) nanoparticle-epoxy composite for advanced lead-free X-ray radiation shielding. ACS Appl Nano Mater 4(7):7471–7478

17. Novoselov KS, Mishchenko A, Carvalho A, Castro Neto AH (2016) 2D materials and van der Waals heterostructures. Science 353(6298):aac9439. https://doi.org/10.1126/science.aac9439
18. Manzeli S, Ovchinnikov D, Pasquier D, Yazyev OV, Kis A (2017) 2D transition metal dichalcogenides. Nat Rev Mater 2(8):1–15. https://doi.org/10.1038/natrevmats.2017.33
19. Das S, Kim M, Lee JW, Choi W (2014) Synthesis, properties, and applications of 2-D materials: a comprehensive review. Crit Rev Solid State Mater Sci 39(4):231–252. https://doi.org/10.1080/10408436.2013.836075
20. Wang J, Zhang Z, Zhu J, Tian M, Zheng S, Wang F, Wang L (2020) Ion sieving by a two-dimensional Ti3C2T x alginate lamellar membrane with stable interlayer spacing. Nat Commun 11(1):3540
21. Ares P, Novoselov KS (2022) Recent advances in graphene and other 2D materials. Nano Mater Sci 4(1):3–9. https://doi.org/10.1016/j.nanoms.2021.05.002
22. Hammond PT (2004) Form and function in multilayer assembly: New applications at the nanoscale. Adv Mater 16(15):1271–1293. https://doi.org/10.1002/adma.200400760
23. Pavlou C, Pastore Carbone MG, Manikas AC, Trakakis G, Koral C, Papari G, Galiotis C (2021) Effective EMI shielding behaviour of thin graphene/PMMA nanolaminates in the THz range. Nat Comm 12(1):4655. https://doi.org/10.1038/s41467-021-24970-4
24. Vogl T et al (2019) Radiation tolerance of two-dimensional material-based devices for space applications. Nat Commun 10(1):1202
25. Shahzad F, Alhabeb M, Hatter CB, Anasori B, Man Hong S, Koo CM, Gogotsi Y (2016) Electromagnetic interference shielding with 2D transition metal carbides (MXenes). Science 353(6304):1137–1140. https://doi.org/10.1126/science.aag2421
26. Yun T, Kim H, Iqbal A, Cho YS, Lee GS, Kim MK, Koo CM (2020) Electromagnetic shielding of monolayer MXene assemblies. Adv Mater 32(9):1906769. https://doi.org/10.1002/adma.201906769
27. Lee SH, Kang D, Oh IK (2017) Multilayered graphene-carbon nanotube-iron oxide three-dimensional heterostructure for flexible electromagnetic interference shielding film. Carbon 111:248–257. https://doi.org/10.1016/j.carbon.2016.10.003
28. Bhattacharjee Y, Arief I, Bose S (2017) Recent trends in multilayered architectures towards screening electromagnetic radiation: challenges and perspectives. J Mater Chem C 5(30):7390–7403. https://doi.org/10.1039/c7tc02172k
29. Nine MJ, Yu L, Pereira AL, Batmunkh M, Hassan K, Santos AM, Losic D (2022) Laminated antimonene as an alternative and efficient shielding strategy against X-ray radiation. Appl Mater Today 29:101566
30. Yu L, Yap PL, Santos AM, Tran DN, Losic D (2023) Lightweight polyester fabric with elastomeric bismuth titanate composite for high-performing lead-free X-ray shielding. Radiat Phys Chem 205:110726
31. Hassan K, Stanley N, Tung TT, Yap PL, Rastin H, Yu L, Losic D (2021) Extrusion-printed CNT–graphene sensor array with embedded MXene/PEDOT: PSS heater for enhanced NO2 sensing at low temperature. Adv Mater Interfaces 8(24):1. https://doi.org/10.1002/admi.202101175
32. Li Z, Zhou W, Zhang X, Gao Y, Guo S (2021) High-efficiency, flexibility and lead-free X-ray shielding multilayered polymer composites: Layered structure design and shielding mechanism. Sci Rep 11(1):4384. https://doi.org/10.1038/s41598-021-83031-4

Authors and Affiliations

Le Yu[1] · Md J. Nine[1] · Tran T. Tung[1] · Ana L. C. Pereira[1,2] · Kamrul Hassan[1] · Diana Tran[1] · Alexandre Santos[3,4,5] · Dusan Losic[1]

✉ Dusan Losic
dusan.losic@adelaide.edu.au

[1] School of Chemical Engineering and Advanced Materials, The University of Adelaide, Adelaide, SA 5005, Australia

[2] School of Applied Sciences, University of Campinas (UNICAMP), Limeira 13484-350, Brazil

[3] School of Physics, Chemistry and Earth Sciences, University of Adelaide, Adelaide, South Australia 5005, Australia

[4] Australian Bragg Centre for Proton Therapy and Research, Adelaide, South Australia 5000, Australia

[5] Department of Medical Physics, Royal Adelaide Hospital, Adelaide, South Australia 5000, Australia